Journal of Luminescence 131 (2011) 874–879

Contents lists available at ScienceDirect

Journal of Luminescence

journal homepage: www.elsevier.com/locate/jlumin

Synthesis of zinc oxide microrods and nano-fibers with dominant exciton emission at room temperature

F. Ramos-Brito [a,*], C. Alejo-Armenta [a], M. García-Hipólito [b], E. Camarillo [c], J. Hernández A [c], C. Falcony [d], H. Murrieta S [c]

[a] Laboratorio de Materiales Optoelectrónicos del Centro de Ciencias de Sinaloa, Ave. de las Américas 2771 Col. Villa Universidad 80010, Culiacán, Sinaloa, México
[b] Departamento de Materiales Metálicos y Cerámicos, Instituto de Investigaciones en Materiales, Universidad Nacional Autónoma de México, AP 70-360, Coyoacán 04510, DF, México
[c] Instituto de Física, Universidad Nacional Autónoma de México, AP 20-364, Alvaro Obregón 01000, DF, México
[d] Departamento de Física, CINVESTAV-IPN, AP 14-740, 07000, DF, México

ARTICLE INFO

Article history:
Received 20 August 2008
Received in revised form
22 December 2010
Accepted 24 December 2010
Available online 31 December 2010

Keywords:
ZnO
Microrods
Nano-fibers
Enhanced UV-emission

ABSTRACT

Employing a simple chemical synthesis method, hexagonal-shaped zinc oxide microrods and zinc oxide nano-fibers were deposited on pyrex-glass and aluminum substrates, respectively. Both kinds of deposits showed zincite crystalline phase with lattice parameters: $a=3.2498$ Å and $c=5.2066$ Å. Microrods showed very uniform wide and large sizes of around 1 and 10 μm, respectively. Both deposits were homogeneous over all substrate surfaces. Microrods and nano-fibers resulted with good optical quality and with preferential crystalline growth in [1 0 1 0] and [0 0 0 1] directions. The principal optical characteristics for both microrods and nano-fibers were: a) room-temperature photo and cathodo-luminescent spectra with strong exciton emission centered around 390 nm and with FWHMs around 125 and 160 meV, respectively, b) poor photo and cathode-luminescent emissions in the visible region of the electromagnetic spectrum, c) energy band gap of 3.32 eV, d) good emission efficiency supported by the not-required high energy densities to obtain strong exciton emission and e) good ZnO stoichiometry endorsed by photoluminescent results. These characteristics make of these microrods and nano-fibers good for potential photonic applications.

1. Introduction

Zinc oxide, ZnO, has always been considered one of the most important semiconductors due to its physical and/or chemical properties and the consequent multiple applications that it has, such as: antireflection coatings, transparent conducting films (as electrodes in solar cells), gas sensors, varistors, surface acoustics wave devices and electro- and photo-luminescent devices. Recently ZnO nanostructures have attracted much attention due to their potential applications in field emission displays [1,2] high efficient optoelectronic devices [3–7], UV laser technology at room-temperature [3,8], phosphors [9–11], photo-catalysis [12], electromechanical coupled sensors and transducers [13,14], spintronics [15,16], super-hydrophobicity and super-hydrophilicity sufaces [17,18],cosmetics [19], etc.

ZnO is a direct band-gap semiconductor with wide band-gap energy (~3.37 eV) at room temperature and a very large exciton binding energy of about 59 meV, which allows for more efficient excitonic emission at higher temperatures [20–22] better than other very important semiconductors such as: GaSb, Ge, GaAs, ZnTe, Si, ZnSe, GaP, GaN, CdS and ZnS with exciton binding energies of: 1.6, 4.15, 4.2, 12, 14.7, 17, 21.5, 25, 28 and 40 meV, respectively. This makes ZnO suitable for short wavelength optoelectronic devices based on excitonic effects that work at room temperature and above. The large ZnO exciton binding energy makes this material an attractive candidate for room-temperature lasing [3,23]; in addition ZnO in low dimensional nanostructured forms offers the possibility of further improving lasing conditions due to quantum confinement effects [3,23].

Typical photoluminescent (PL) emission spectrum for zinc oxide shows an emission peak in the near UV region and a broad band in the visible region. Recent studies on ZnO are focused to obtain strong ultraviolet emission and minimize the emission in the visible region in order to increase the optical quality of the ZnO for future applications as a lasing material [24–27]. The near-band-edge (UV-PL peak) is commonly observed in the range 370–390 nm, which corresponds to energies in a range 3.2–3.35 eV [24–28]; this is believed to result from an excitonic type recombination where free exciton process is dominant. The typical visible emission in ZnO

* Corresponding author. Tel.: +52 667 7599000x1185, 1166.
E-mail addresses:
fro_brito@yahoo.com.mx, ramosbritof@gmail.com (F. Ramos-Brito).

0022-2313/$ - see front matter © 2010 Elsevier B.V. All rights reserved.
doi:10.1016/j.jlumin.2010.12.017

is in the blue–green–orange region, which results due to deep energy levels in the forbidden band gap, resulting from structural defects in the crystal lattice [24–27,29–32]. These structural defects act as traps for carriers, and have been mainly attributed to surface defect levels associated with oxygen vacancies, oxygen interstitial, antisite oxygen O_{zn}, zinc vacancies and/or zinc interstitials in the ZnO crystal lattice [29–33].

Up to now, the origin of the visible emission is highly controversial and with numerous hypotheses [32,34], this has been attributed to surface defects as was mentioned before but the nature of these defects is still not fully understood [32,34]. Detailed investigations on the properties of ZnO are required in order to have functional ZnO devices.

The aim of the present manuscript is to evaluate a simple chemical synthesis method to obtain zinc oxide microstructures and/or nanostructures that have predominant ultraviolet emission over visible emission. These ZnO structures could have good possibilities of room-temperature lasing applications. The results show that the synthesis method is appropriate to produce ZnO microrods and nano-fibers structures with predominant ultraviolet emission over visible emission.

Employing the wet chemical synthesis method, rod shaped structures with dimensions of microns and fiber structures with dimensions of nanometers were synthesized. Both structures presented photo- and cathode-luminescence emission spectra without significant contribution in the visible region of the electromagnetic spectrum. The blue–green–orange emission was not present even though emission is very common in ZnO prepared by chemical methods [35]. Precursor materials and the method employed here minimize the structural defects, which maximize the emission centered in the range 370–390 nm associated to exciton processes.

2. Experimental procedures

Zinc oxide deposits were obtained by wet chemical synthesis method [36]. The precursor solution was zinc acetate hydrate 99.99%, Aldrich, (0.032 M) and hexamethylenetetramine 99% and Aldrich (0.032 M) in deionized water (18 M Ω cm). The zinc oxide was grown on aluminum and pyrex-glass substrates. The substrates with $1.0 \times 1.0\ cm^2$ dimensions were immersed in 100 ml of precursor solution at 90 °C for 15 h. Subsequently the deposited zinc oxide was washed with deionized water several times to eliminate residual salts. A Leica Cambridge Stereoscan 440 Scanning Electron Microscope (SEM) equipped with a beryllium window X-ray detector was employed to obtain the morphology of the samples, and their chemical composition (by Energy Dispersive Spectroscopy, EDS). Crystalline structure was analyzed by X-ray diffraction (XRD) using a Broker-axs D8-advance with CuKα radiation at 1.5426 Å. Identification of hexagonal phase and indexing of the peaks for the XRD patterns were carried out using XRD-PDF cards provided by ICCD with associated numbers: 00-036-1451 for zinc oxide, 00-004-0831 for zinc and 00-004-0787 for aluminum. Photoluminescence excitation and emission spectra at room temperature, T_{room}, were recorded using a spectrofluorometer SPEX Fluoro-Max-P. Lamp intensity correction is performed automatically by this instrument that measures the excitation light intensity with an additional photomultiplier tube and performs the correction accordingly before displaying the data. A 10 ns Nd:YAG pulsed laser model Quanta-Ray of Spectra Physics was employed as excitation source to obtain T_{room} and 18 K PL spectra of the samples. A filter was used to reject the 532 and 1064 nm laser lines. The emission spectra were recorded using a conventional setup. The sample was placed in a mobile holder for aligning purpose, which was inside a compressed-helium cryostat of Air Products. The emission was collected perpendicular to the pumping signal. A monochromator, model SpectroPro 2500i of Acton Research Corporation, was used to scan the emission spectrum and then measured using a photomultiplier tube, model R-930 of Hamamatsu, connected to a PC through a Lock-in amplifier, model SR530 of Stanford Research Systems. Both slits of the monochromator were placed at 100 μm. A luminoscope, model ELM-2; MCA of Relion Corporation was employed to obtain Cathodo-Luminescence (CL) measurements; these were obtained in a stainless steel vacuum chamber equipped with a cold cathode electron gun. Samples were placed inside the vacuum chamber and evacuated to 10^{-2} Torr. The emitted light from the sample was coupled to an optical fiber bundle leading to a spectrofluorometer SPEX Fluoro-Max-P. CL spectra were recorded at room temperature. The accelerating voltage of the electron beam was 10 kV and the applied current was kept constant at 0.3 mA. The spot size of the electron beam on the sample surface was approximately 3 mm in diameter. Diffuse reflectance measurements in a range 200–800 nm were carried out by employing an UV–vis–NIR spectrophotometer, model Cary 5000 of VARIAN.

3. Results and discussion

Fig. 1 shows SEM micrographs that are representatives of the surface morphology for zinc oxide deposited on pyrex-glass (ZnO_{glass}) and aluminum substrates (ZnO_{Al}). Fig. 1a, b, and c shows how ZnO_{glass} was conformed by overlapping ZnO microrods. These figures show ZnO microstructures with evident hexagonal crystalline structure and the preference of the material to grow in a well formed rod shape. It is notable that the preferred growth of ZnO is along the *c*-axis [0 0 0 1] direction. In Fig. 1a, three different microstructures can be observed principally: 1) well formed rods (R_W), 2) Two rods with single intersection (R_{SI}) and 3) Multiple rods with single intersection (R_{MI}); these characteristics possibly result from certain differences in the growing processes of the material properly influenced by the local chemical and/or thermodynamic environment, but not by the substrate nature. From Fig. 1b it is possible to observe uniformity in diameters and lengths for R_W, R_{SI} and R_{MI} microstructures and a remarkable predominant existence of R_W over the other two types of microstructures. Diameter and length average values were lower than 1 and 10 μm, respectively. A random inspection over all substrate areas shows how this was uniformly covered by these kinds of microstructures, analogous to the area showed in Fig. 1c. SEM micrographs presented in Fig. 1d

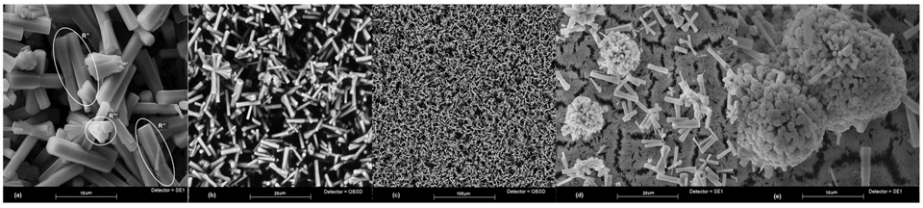

Fig. 1. SEM micrographs that present different magnifications of ZnO_{glass} (a, b and c) and ZnO_{Al} (d and e) samples. R_W—well formed rod, R_{SI}—two rods with single intersection, R_{MI}—microrods with multiple intersections.

and e are representatives of the surface morphology for ZnO_{Al} samples. Three remarkable differences for ZnO_{Al} in relation to ZnO_{glass} can be observed: 1) there is a considerable lower quantity of microrods covering the substrate surface, 2) there is a porous and cracked micro-film deposited over the entire substrate surface that is conformed by nano-fibers of ZnO and 3) another kind of microstructure, besides the microrods, was obtained, which is formed by multiple rods with submicron dimensions emerging in a radial way from a single point. Fig. 1e clearly reveals hexagonal-shaped and submicron dimensions of transversal sections of the microrods that form this microstructure. The morphology of the synthesized ZnO micro-film and the low quantity of microrods per unit area can be appreciated in Fig. 1d. The film formation is a consequence of the reactive nature of the aluminum substrate, which is not the case for pyrex substrate. Therefore aluminum has high efficiency in the film formation process and low efficiency in the microrods growth process as compared to pyrex-glass.

Chemical composition by EDS over an area of approximately $100\,\mu m \times 100\,\mu m$ for ZnO_{glass} resulted in atomic-percent (at%) contents of: oxygen: 51.50 at% and zinc: 48.50 at%; in great accordance with ZnO stoichiometry, which indicates that it is possible to have a majority of the microrods conformed by stoichiometric ZnO. For ZnO_{Al}, the chemical composition analyses by EDS over ZnO film (nano-fibers) and the microstructure formed by multiple rods with submicron dimensions emerging in a radial way from a single point were done, resulting in atomic-percent contents of: O: 79.46 at%, Al: 7.5 at%, Zn: 13.03 at% and O: 70.89 at%, Al: 0.0 at%, Zn: 29.11 at%, respectively. The high content of oxygen in the nano-fibers and into the cited microstructure could indicate a high value of zinc vacancies or interstitial oxygen in their crystalline structures. The EDS analysis corresponding to ZnO nano-fibers was made removing part of the film from the substrate. The removed film presented a thickness of 6 μm.

Fig. 2a shows the XRD pattern for ZnO_{glass}. A hexagonal crystalline structure with lattice parameters of: $a=3.2498$ and $c=5.2066$ were observed. All peaks observed corresponded to hexagonal ZnO without evidence of any other type of crystal phase or another material. The major intensity of the peaks centered at $2\theta=31.8^\circ$ and 34.5° show a preferred growth in [1 0 1 0] and [0 0 0 1] directions, in agreement with the microrods observed in SEM micrographs. Fig. 2b shows the XRD pattern obtained for ZnO_{Al}. A wide band from 6° to 24° 2θ values was observed; it is probably associated to amorphous compounds (Al–Zn–O) in the ZnO film. The peaks with superior intensity centered at $2\theta=38.5^\circ$, 44.8° and 65.1° correspond to the employed cubic-aluminum substrate. The peaks labeled by & symbol were associated to ZnO with hexagonal crystalline structure and lattice parameters of: $a=3.2498$ Å and $c=5.2066$ Å. The major intensity of the peaks centered at $2\theta=31.8^\circ$ and 34.4° show a preferred growth in [1 0 1 0] and [0 0 0 1] directions. This is in agreement with the three kinds of microstructures observed in SEM micrographs (Fig. 1d) and indicates a preferred growth of the film (nano-fibers) in [1 0 1 0] and [0 0 0 1] directions.

In Fig. 2b there are two peaks centered at $2\theta=33.7^\circ$ and 60.3° (labeled with the symbol #), which cannot be associated to ZnO or the presence of Al doped ZnO; this is because studies on Al heavy-doped zinc oxide do not show the apparition of these two peaks [37]. Furthermore, these studies do not show additional peaks other than the peaks associated with ZnO. Choppali and Gorman [38] found similar peaks in ZnO films deposited on sapphire and they associated the peaks to the formation of a spinel phase, $ZnAl_2O_4$, at the substrate and film interface, but this was only present when films were subjected to a 1273 K annealing process. In this work, the samples were not subjected to any type of annealing process. Future studies in this direction are needed to elucidate the origin of these two peaks in the XRD pattern for ZnO_{Al}.

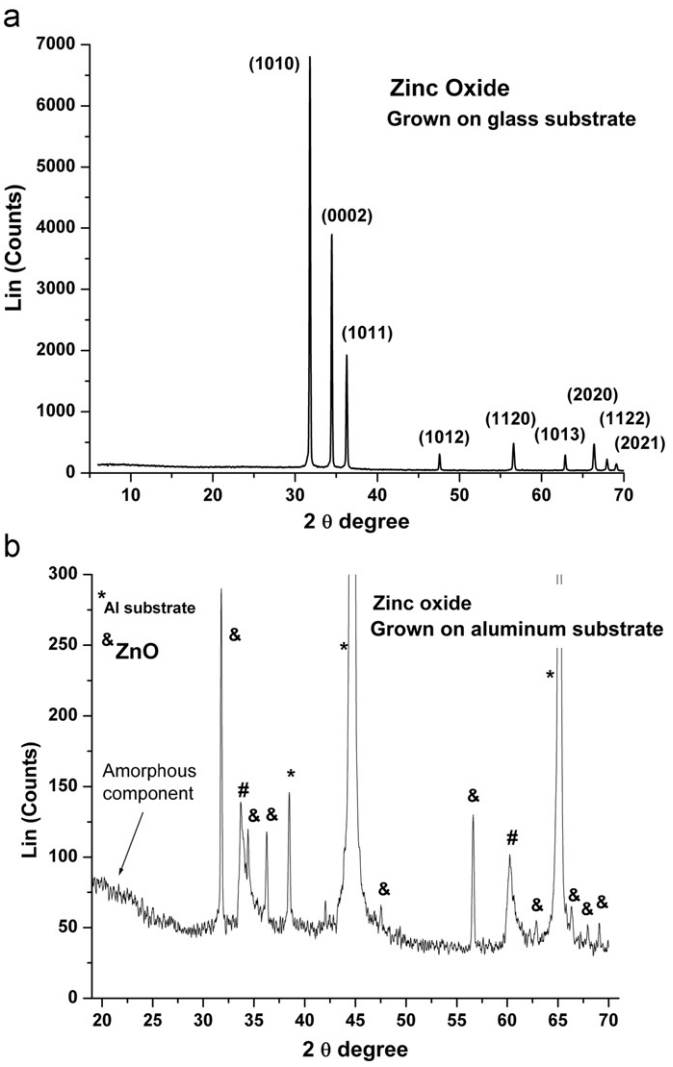

Fig. 2. XRD pattern for (a) ZnO_{glass} and (b) ZnO_{Al} samples.

Fig. 3 shows the results obtained by diffuse reflectance spectroscopy of ZnO_{glass}. In the interest of the signal coming from the substrate, diffuse reflectance spectrum of pyrex-glass was measured. Microrods were deposited over one of the two possible substrate surfaces; in this sense, covered-face spectrum in Fig. 3 corresponds to diffuse reflectance measured over the substrate surface where microrods rest and uncovered-face spectrum to the opposite surface. Considering the three spectra presented in Fig. 3, the great absorption starting at 405 nm and having a maximum at 373 nm and the low intensity peak centered at 230 nm were attributed to ZnO microrods. The absorption at 373 nm was associated with the near band edge absorption for zinc oxide and suggests an energy band gap of 3.32 eV. The absorption at 230 nm (5.4 eV) corresponds to the absorption of O^{2-} 2p electrons in the valence band [39]. The inset in Fig. 3 shows the diffuse reflectance spectrum for ZnO_{Al}. There are two things to highlight, one is the band tail absorption that starts at 550 nm and the other is the intense absorption at 373 nm. The last is associated to the near band edge absorption for zinc oxide, as was mentioned before for ZnO_{glass}. Both samples, ZnO_{glass} and ZnO_{Al}, show band tail absorption that was associated to defects in the crystalline structure of ZnO. This is in agreement with the emission bands that were centered in the visible region of the photo and cathode-luminescent emission spectra (Figs. 4, 5 and 8) obtained for ZnO_{glass} and ZnO_{Al} samples.

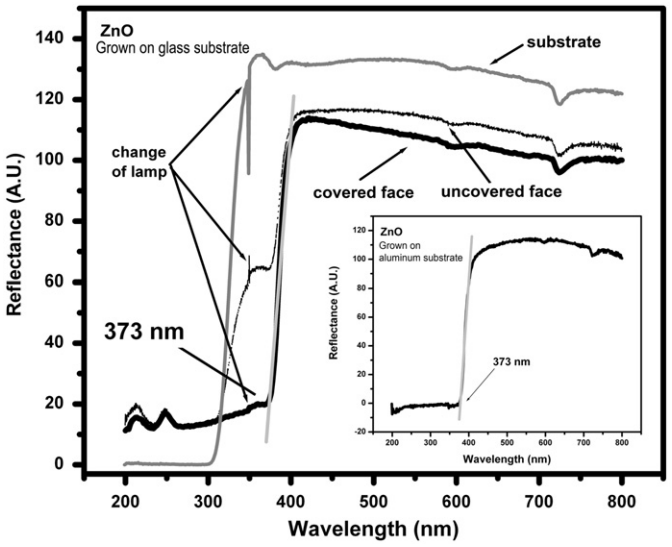

Fig. 3. Diffuse reflectance spectrum for ZnO_{glass}—bold solid line. Gray curve represents diffuse reflectance spectrum of the pyrex-glass substrate. Solid line represents the diffuse reflectance spectrum of ZnO_{glass} when it is measured on the opposite face to where ZnO was deposited. The inset of the figure shows the diffuse reflectance spectrum for ZnO_{Al}.

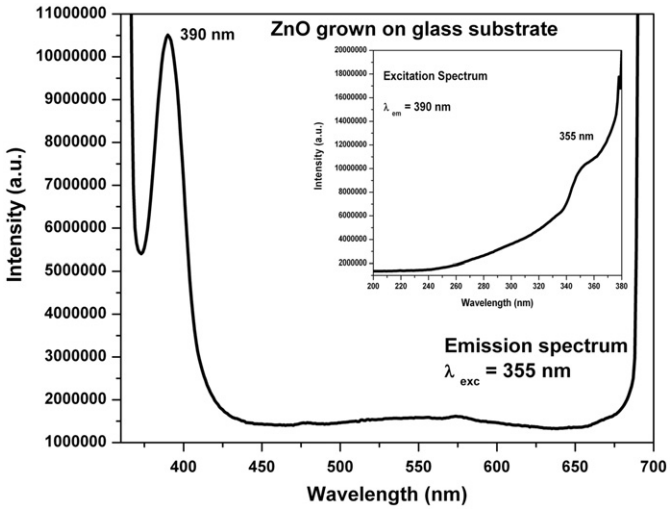

Fig. 4. Room-temperature photoluminescent emission spectrum for ZnO_{glass}. Emission spectrum was recorded using light of 355 nm as excitation source. Inset shows the excitation spectrum of ZnO_{glass} by selecting 390 nm to fix the emission wavelength.

Figs. 4 and 5 show the T_{room} PL emission and excitation spectra for ZnO_{glass} and ZnO_{Al}, respectively. They were obtained by employing a spectrofluorometer SPEX Fluoro-Max-P. Both PL emission spectra were obtained using light of 355 nm as excitation source. The ZnO_{glass} emission spectrum shows an intense peak centered at 390 nm, which was associated to intrinsic exciton emission of ZnO. An almost imperceptible emission band centered at 550 nm is also observed; this was associated to crystalline defects of ZnO. The inset of the Fig. 4 shows the excitation spectrum of ZnO_{glass} for an emission wavelength of 390 nm. The spectrum shows an excitation band at 355 nm, which overlaps the near band edge absorption. This may indicate a preferred excitation path to maximize the intrinsic exciton emission of ZnO_{glass}. Analogous to ZnO_{glass}, ZnO_{Al} shows an emission spectrum that has an intense peak centered at 389 nm, as can be seen in Fig. 5. This was associated to intrinsic exciton emission of ZnO. The broad

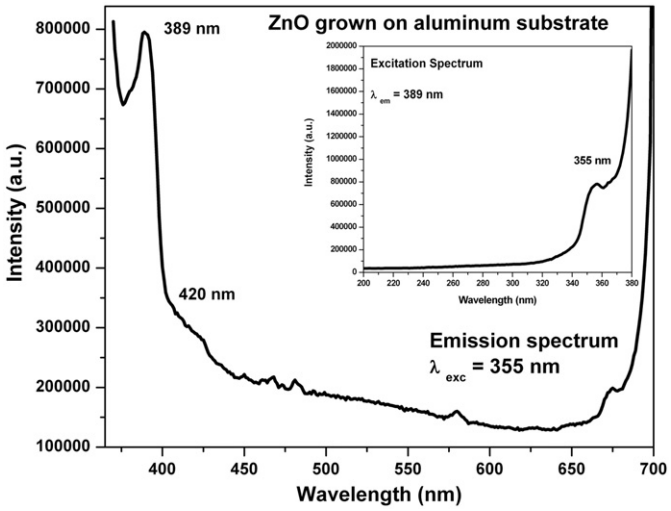

Fig. 5. Room-temperature photoluminescent emission spectrum for ZnO_{Al}. Emission spectrum was recorded using light of 355 nm as excitation source. Inset shows the excitation spectrum of ZnO_{Al} by selecting 389 nm to fix the emission wavelength.

asymmetric shape of the exciton emission peak in ZnO_{Al} is attributed to: a) the coupling of free excitons to the replicas of LO phonons [38] and b) an emission band centered at 420 nm, which was associated to defects in the crystalline structure of ZnO and overlap the exciton emission band. The inset of Fig. 5 shows the excitation spectrum of ZnO_{Al} for an emission wavelength of 389 nm. The spectrum shows how ZnO_{Al} prefers light of 355 nm to improve his intrinsic exciton emission. Figs. 4 and 5 show how, at relatively low energy densities, the relative intensity of the exciton emission is strong and the contribution of the crystalline defects in the emission spectra of ZnO_{glass} and ZnO_{Al} is poor, indicating good exciton emission efficiency. It means that a great percent of electron–hole pairs formed are easily changed into excitons, which is not surprising if the high binding energy of the exciton, 60 meV, is considered, but, on the other hand, a strong exciton emission measured at T_{room}, when a lamp is employed as excitation source, is rarely showed by ZnO samples that were synthesized by chemical methods. This is due to a dominant effect of emission coming from the presence of defects in its crystalline structure over the exciton emission; this is one reason why most authors use an intense excitation source (laser) to maximize the conversion of electron–hole pairs into exciton emission [40].

Fig. 6 shows the PL emission spectra for ZnO_{glass} using the 355 nm laser line of Nd:YAG laser as excitation source. The spectra were recorded at two different temperatures: 18 K (a) and T_{room}=290K (b). A strong emission centered at 388 nm for T_{room} and 373 nm for T=18 K, was observed. The inset of the figure does not show evidence of the existence of peaks in the visible region. The missing visible emission reveals high optical quality of the obtained microrods. The red shift of the exciton peak, when temperature increases, is due to the widening of the near band edge associated to the phonon contribution. ZnO_{glass} shows FWHM values for exciton emission peaks of: 46 meV: 18 K and 129 meV: 290 K.

Fig. 7 shows the PL emission spectra for ZnO_{Al} using the 355 nm laser line of Nd:YAG laser as excitation source. The spectra were recorded at two different temperatures: 18 K (a) and T_{room}=290 K (b). A strong emission centered at 386 nm for T_{room} and 370 nm for T=18 K, were observed. The inset of the figure does not show evidence of emission peaks in the visible region, but when the slits of the monochromator were increased from 100 to 750 μm (spectrum labeled with θ), the emission peaks associated to

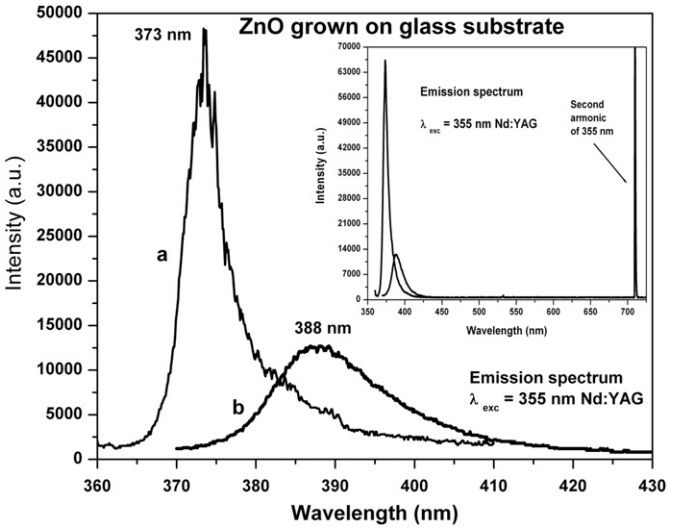

Fig. 6. Photoluminescent emission spectra for ZnO_{glass} recorded at two different temperatures: (a) 18 K and (b) 290 K. Emission spectra were recorded using the 355 nm laser line of Nd:YAG laser as excitation source. Inset shows the emission spectra recorded in a range 375–750 nm.

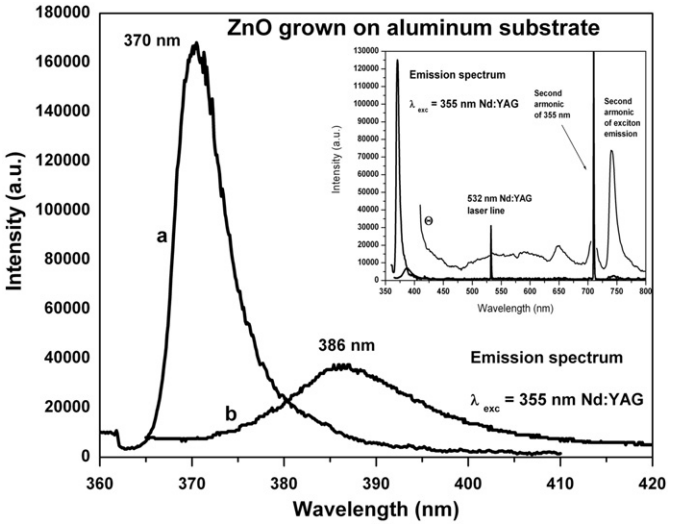

Fig. 7. Photoluminescent emission spectra for ZnO_{Al} recorded at two different temperatures: (a) 18 Kelvin and (b) 290 Kelvin. Emission spectra were recorded using the 355 nm laser line of Nd:YAG laser as excitation source. Inset shows the emission spectra recorded in a range 375–750 nm. The emission spectrum labeled with θ symbol was recorded after the two monochromator slits were increased from 100 to 750 μm.

crystalline defects appear; this corroborates the poor existence and/or poor contribution of the defects in the emission spectrum and may indicate the existence of a preferred de-excitation path that improves exciton emission. The missing visible emission reveals high optical quality of the obtained nano-fibers. ZnO_{Al} shows FWHM values for exciton emission peaks of: 56 meV: 18 K and 121 meV: 290 K.

Fig. 8 shows the T_{room} CL emission spectra for ZnO_{glass} and ZnO_{Al}. Both samples show strong exciton emission and poor visible emission. The strong exciton emission under high energy electron excitation indicates the relatively poor existence of crystalline defects for both samples and is in agreement with the high optical quality of the samples. The relative low intensity of the emission bands, 570 nm for ZnO_{glass} and 500 nm for ZnO_{Al}, indicates the presence of crystalline defects in microrods and nano-fibers, and

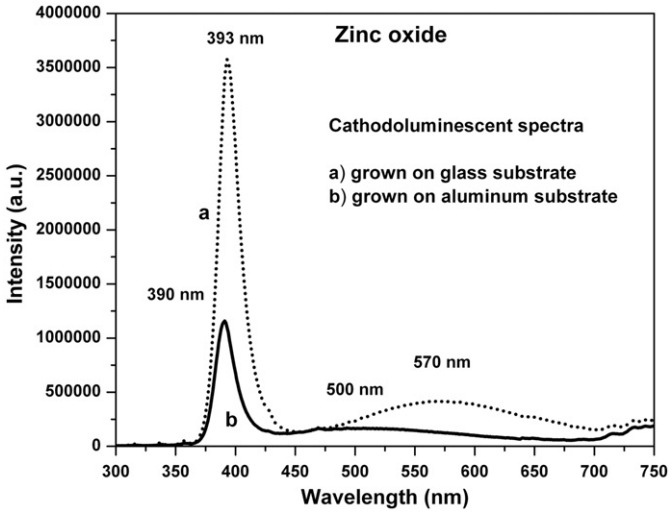

Fig. 8. Cathodo-luminescent emission spectra for (a) ZnO_{glass} and (b) ZnO_{Al} samples. The accelerating voltage of the electron beam was 10 kV and the applied current was kept constant at 0.3 mA. The spot size of the electron beam on the sample surface was approximately 3 mm in diameter.

corroborates the existence of a preferred excitation wavelength (355 nm) to improve the excitation emission. The blue shift of the emission band associated to crystalline defects in ZnO_{Al} is probably due to the different nature of the defects in ZnO_{Al} as compared with defects in ZnO_{glass}.

4. Conclusions

Employing a simple chemical synthesis method, hexagonal-shaped zinc oxide microrods and zinc oxide nano-fibers were deposited on pyrex-glass and aluminum substrates, respectively. Both deposits were homogeneous over all substrate surfaces. Microrods and nano-fibers resulted with good optical quality and with preferential crystalline growth in [1 0 1 0] and [0 0 0 1] directions. The principal optical characteristics for both, microrods and nano-fibers were: a) room-temperature photo- and cathodo-luminescent spectra with strong exciton emission centered around 390 nm and with FWHMs around the 125 and 160 meV, respectively, b) poor photo- and cathode-luminescent emissions in the visible region of the electromagnetic spectrum, c) energy band gap of 3.32 eV, d) good emission efficiency supported by the not-required high energy densities to obtain strong exciton emission and e) good ZnO stoichiometry endorsed by photoluminescent results. These characteristics make of these microrods and nano-fibers good for potential photonic applications.

The ZnO_{glass} sample was merely composed of a pile of microrods and there was no evidence of any other kind of microstructure. The micrographs exhibit a uniform distribution of these entities over the surface, very uniform wide and large sizes of around 1 and 10 μm, respectively; and high microrod-formation rate. Photoluminescence, XRD, micrographs and EDS results strongly suggest microrods conformed by stoichiometric ZnO.

The ZnO_{Al} sample was composed of three kinds of microstructures: a) microrods, b) microstructures formed by multiple rods with submicron dimensions emerging in a radial way from a single point and c) a micro-film conformed by nano-fibers. The population of the first two microstructures over the substrate surface was relatively low compared with the micro-film that was deposited over the entire substrate surface. The film was homogeneously deposited. The photoluminescence and XRD studies obtained from the film are in agreement with a stoichiometric

ZnO, but EDS studies were not enough to have information about its stoichiometry. More studies, probably the Rutherford Back Scattering study, are necessary to elucidate the chemical composition of the film.

The wet chemical method was appropriated for deposition of microrods and nano-fibers with the desired optical properties for its possible application in photonics. Due to the simplicity of the method and the lower quantity of structural defects induced on ZnO structures by this technique, the study of the optical properties of ZnO structures as a function of its physical dimensions can be done in the future. This should work to find the critical dimension sizes of the ZnO structures that maximize its exciton emissions and minimize their visible emission originated by structural defects.

Acknowledgments

The authors thank Lorena Uriarte, Omar Novelo, Leticia Baños, Carmina Díaz and Laura Martínez for technical support provided, Universidad Nacional Autónoma de México under its postdoctoral fellowship program, CONACYT CB-2006-1-J1-I0002-57809 (México) and CECyT (Sinaloa-México) for the financial grant for this investigation.

References

[1] C. Liu, J.A. Zapien, Y. Yao, X. Meng, C.S. Lee, S. Fan, Y. Lifshitz, S.T. Lee, Adv. Mater. 15 (2003) 838.
[2] X.D. Bai, E.G. Wang, P.X. Gao, Z.L. Wang, Nano Lett. 3 (2003) 1147.
[3] P. Yang, H. Yan, S. Mao, R. Russo, J. Johnson, R. Sayakally, N. Morris, J. Pham, R. He, H. Choi, Adv. Funct. Mater. 12 (2002) 323.
[4] Ü. Özgür, Y.I. Alivov, C. Liu, M. Reshchikov, S. Dooan, V. Avrutin, S.-J. Cho, H. Morkoc, J. Appl. Phys. 98 (2005) 041301.
[5] L.L. Zhang, C.X. Guo, J.G. Chen, J.T. Hu, Chin. Phys. 14 (2005) 586.
[6] R.D. Zu, W.P. Zheng, Z.L. Wang, Adv. Funct. Mater. 13 (2003) 9.
[7] X.Y. Kong, Y. Ding, R.S. Yang, Z.L. Wang, Science 303 (2004) 1348.
[8] J.C. Johnson, H. Yan, R.D. Schaller, L.H. Haber, R.J. Sayakally, P. Yang, J. Phys. Chem. B 105 (2001) 11387.
[9] A. Pfahnl, J. Electrochem. Soc. 109 (1962) 502.
[10] C.T. Troy, Photonics Spectra 31 (1997) 34.
[11] S.A. Studenikin, N. Golego, M. Cocivera, J. Appl. Phys. 84 (1998) 2287.
[12] J.S. Jang, Ch-J. Yu, S.H. Choi, S.M. Ji, E.S. Kim, J.S. Lee, J. Catal. 254 (2008) 144.
[13] M.S. Arnold, P. Avouris, Z.W. Pan, Z.L. Wang, J. Phys. Chem. B 107 (2003) 659.
[14] E. Comini, G. Faglia, G. Sberveglieri, Z.W. Pan, Z.L. Wang, Appl. Phys. Lett. 81 (2002) 1869.
[15] T. Dietl, Semicond. Sci. Technol. 17 (2002) 377.
[16] K. Sato, H. Katayama-Yoshida, Jpn. J. Appl. Phys. 39 (part 2, no. 63) (2000) L555.
[17] M. Guo, P. Diao, S. Cai, Thin Solid Films 515 (2007) 7162.
[18] X. Feng, L. Feng, M. Jin, J. Zhai, L. Jiang, D. Zhu, J. Am. Chem. Soc. 126-1 (2004) 63.
[19] Cosmetics formulation comprising ZnO nanoparticles USPTO Patent Application 20050255057.
[20] Y. Segawa, A. Ohtomo, M. Kawasaki, H. Koinuma, Z.K. Tang, P. Yu, G.K.L. Wong, Phys. Status Solidi (b) 202 (1997) 669.
[21] P. Yu, Z.K. Tang, G.K.L. Wong, M. Kawasaki, A. Ohtomo, H. Koinuma, Y. Segawa, Solid State Commun. 103 (1997) 459.
[22] Z.K. Tang, G.K.L. Wong, P. Yu, M. Kawasaki, A. Ohtomo, H. Koinuma, Y. Segawa, Appl. Phys. Lett. 72 (1998) 3270.
[23] M.H. Huang, S. Mao, H. Feick, H. Yan, Y. Wu, H. Kind, E. Weber, R. Russo, P. Yang, Science 292 (2001) 1897.
[24] Y. Fang, Q. Pang, X. Weng, J. Wang, S. Yang, Small 2 (2006) 612.
[25] M.-K. Li, D.-Z. Wang, S. Ding, Y.-W. Ding, J. Liu, Z.-B. Liu, Appl. Surf. Sci. 253 (2007) 4161.
[26] M. Izaki, T. Shinagawa, H. Takahashi, J. Phys. D: Appl. Phys. 39 (2006) 1481.
[27] Y. Segawa, H.D. Sun, T. Makino, M. Kawasaki, H. Koinuma, Phys. Status Solidi (a) 192 (2002) 14.
[28] J.Y. Park, H. Oh, J.-J. Kim, S.S. Kim, J. Cryst. Growth 287 (2006) 145.
[29] H. Gao, F. Yan, J. Li, Y. Zeng, J. Wang, J. Phys. D: Appl. Phys. 40 (2007) 3654.
[30] K.K. Kim, N. Koguchi, Y.W. Ok, T.Y. Seong, S.J. Park, Appl. Phys. Lett. 84 (2004) 3810.
[31] H.Q. Wang, G.Z. Wang, L.C. Jia, C.J. Tang, G.H. Li, J. Phys. D: Appl. Phys. 40 (2007) 6549.
[32] H.S. Kang, J.W. Kim, S.H. Lim, H.W. Chang, G.H. Kim, J.H. Kim, S.Y. Lee, Superlattices and Microstruct. 39 (2006) 193.
[33] K. Vanheusden, W.L. Warren, C.H. Seager, D.R. Tallant, J.A. Voigt, B.E. Gnade, J. Appl. Phys. 79 (1996) 7983.
[34] A.B. Djurisic, Y.H. Leung, Adv. Funct. Mater. 14 (2004) 856.
[35] Y.-Y. Li, Y.-X. Li, Y.-L. Wu, W. Sun, J. Lumin. 126 (2007) 177.
[36] L. Vayssieres, K. Keis, S.-E. Lindquist, A. Hagfeldt, J. Phys. Chem. B 105 (2001) 3350;
D. Bera, L. Qian, S. Sabui, S. Santra, P. Holloway, Opt. Mater. 30 (2008) 1233.
[37] L.J. Li, H. Deng, L.P. Dai, J.J. Chen, Q.L. Yuan, Y. Li, Mater. Res. Bull. 43 (2008) 1456.
[38] U. Choppali, B.P. Gorman, J. Lumin. 128 (2008) 1641.
[39] Ch. Shi, Z. Fu, Ch. Guo, X. Ye, Y. Wei, J. Deng, J. Shi, G. Zhang, J. Electron Spectrosc. Relat. Phenom. 101–103 (1999) 629.
[40] A.B. Djurisic, W.M. Kwok, W.K. Chan, D.L. Phillips, Y.H. Leung, M.H. Xie, Y.H. Chen, C.L. Wu, S. Gwo, J. Appl. Phys. 99 (2006) 033517.